ACS SENSORS

pubs.acs.org/acssensors

Article

Plasmonic MOF Thin Films with Raman Internal Standard for Fast and Ultrasensitive SERS Detection of Chemical Warfare Agents in Ambient Air

Marta Lafuente, Sarah De Marchi, Miguel Urbiztondo, Isabel Pastoriza-Santos,* Ignacio Pérez-Juste, Jesús Santamaría, Reyes Mallada,* and María Pina

Cite This: *ACS Sens.* 2021, 6, 2241−2251

Read Online

ACCESS | Metrics & More | Article Recommendations | Supporting Information

ABSTRACT: Surface-enhanced Raman scattering (SERS) is a powerful spectroscopic technique for selective detection and quantification of molecules at extremely low concentrations. However, practical SERS applications for gaseous chemicals with small cross section is still in its early stages. We herein report a plasmonic-sorbent thin-film platform with integrated Raman internal standard with outstanding SERS sensing capabilities for chemical warfare agents (CWA) simulants. The thin film is constituted of close-packed core−shell Au@Ag nanorods individually encapsulated within a ZIF-8 framework (Au@Ag@ZIF-8). While the Au@Ag nanoparticles amplify the Raman signal of molecules located near their surface, the ZIF-8 framework plays a key role in the trapping of the dimethyl methylphosphonate (DMMP) or 2-chloroethyl ethyl sulfide (CEES) from the gas phase as well as Raman internal standard. The underlying adsorption mechanism of the molecules within the ZIF-8 framework as well as the interaction between DMMP and Ag surface are investigated by computational simulations. Outstanding SERS sensing capabilities of Au@Ag@ZIF-8 thin films, in terms of response time, quantification limit, reproducibility, and recyclability, are demonstrated for dimethyl methylphosphonate (DMMP) and 2-chloroethyl ethyl sulfide (CEES), selected as CWA simulants of sarin gas and mustard gas, respectively. A limit of detection (LOD) of 0.2 ppbV is reported for DMMP. Additionally, experiments performed with portable Raman equipment detect 2.5 ppmV for DMMP in ambient air and 76 ppbV for CEES in N_2, with response times of 21 and 54 s, respectively. This proof of concept opens the door for handheld SERS-based gas sensing at ultralow concentrations in practical applications, such as homeland security, critical infrastructure protection, chemical process monitoring, or personalized medicine.

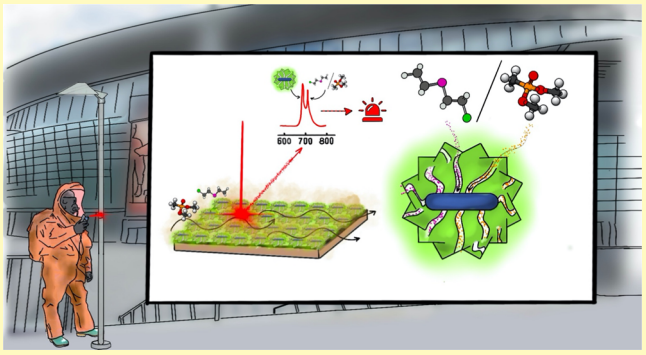

KEYWORDS: *ZIF8, core−shell, surface-enhanced Raman scattering (SERS), DFT and Monte Carlo simulations, ultratrace detection, toxic gases, portable Raman*

Surface-enhanced Raman scattering (SERS) is based on the enhancement of the Raman signal of a molecule close to or in contact with a plasmonic nanostructured surface. The tremendous progress in the fundamental SERS research has shown that this spectroscopic technique one of the most sensitive tools currently available for detection, identification, and quantification of single or multiple molecules even at ultralow concentrations. Nevertheless, as stated in a comprehensive perspective of SERS from worldwide experts recently published, several issues and challenges need to be faced.[1] In fact, reliable proofs of SERS performance in relevant applications, preferentially with nonresonant molecules, are still needed for this technique to become a conventional analytical tool on the market. On the other hand, its high expectations have triggered intense technological progress in Raman-related instrumentation. The use of handheld Raman equipment has been described in the recent literature for on-field SERS analysis in forensic science,[2] monitoring of air volatile organic compounds (VOCs),[3] and detection of nerve agents.[4]

Identification, quantification, and monitoring of hazardous and toxic substances in environmental air are crucial for controlling air pollutants, prevent environmental disasters, evaluate scenarios, and alert the population of possible terrorist attacks with chemical weapons. Neurotoxic agents are easier to synthesize and the most toxic chemical weapons. In general,

Received: January 27, 2021
Accepted: May 7, 2021
Published: May 27, 2021

https://doi.org/10.1021/acssensors.1c00178
ACS Sens. 2021, 6, 2241−2251

Scheme 1. Schematic Overview of the Fabrication of Au@Ag@ZIF-8 SERS Substrates for Gas-Phase Detection of Neurotoxic Agents in Air and the Role of the ZIF-8 Pores in That Detection

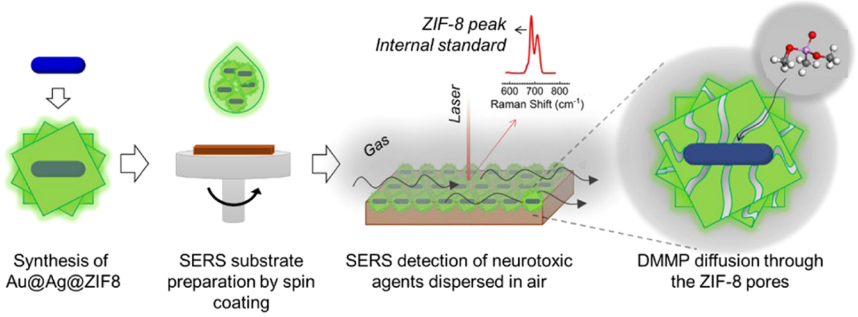

rapid, reliable, ultrasensitive, and fieldable detection of neurotoxic agents in the air becomes imperative for a proper hazard assessment and intervention. The US Environmental Protection Agency (EPA) establishes the Acute Exposure Guideline Levels (AEGLs) that describe the human health effects for periods of exposure to airborne chemicals ranging from 10 min to 8 h. For each exposure period, three levels (AEGL-1, AEGL-2, and AEGL-3) are distinguished as a function of the toxic effects. These threshold exposure values are used as a reference by emergency responders to define tactics and technological tools. Thus, while AEGL-1 refers to nondisabling, transient, and reversible effects, AEGL-3 indicates life-threatening health effects or death. In the case of Sarin gas, the AEGL-1 and AEGL-3 values, for 10 min of exposure, are as low as 1.2 and 64 ppbV, respectively.[5]

In the particular case of gaseous detection at ultralow concentrations, one of the major challenges is the poor sensitivity arising from the low number of molecules available per unit volume. Apart from sensitivity, in sensing toxic gaseous molecules, the selectivity and response time are the most important requirements to ensure public safety.[1] Focused on SERS detection and taking into account the small cross section[6] and lack of strong affinity to the metallic substrate of numerous CWAs, it is crucial to develop SERS sensing platforms with outstanding performances in terms of selectivity, sensitivity, and reliability.[7,8] Regarding the SERS detection of gas-phase toxic agents at low concentrations, i.e., below 5 ppmV, several specific interactions between toxic molecules and plasmonic nanostructures have been already reported. Lauridsen et al. demonstrated, taking advantage of the interaction between the analyte and Au surface, the direct detection of 5 ppmV gaseous hydrogen cyanide in nitrogen using dense-packed silicon pillars coated with gold.[9] We reported the detection of the nerve agent simulant dimethyl methylphosphonate (DMMP) with a theoretical limit of detection (LOD) of 130 ppbV taking advantage of the hydrogen-bonding interaction between DMMP and citrate-stabilized Au nanoparticles.[10] We also showed that the specific interaction of DMMP through the PO_3 umbrella with Ag nanoplates allowed the detection of 2.5 ppmV of gaseous DMMP with portable Raman equipment.[4] Kim et al. investigated the detection of NO_2 in ambient air using three-dimensional (3D) multilayered Ag nanowires (NWs) coated with thin Au layers.[11] The specific binding of NO_2 onto the Au surface together with the high density of hotspots generated by the interconnected 3D structures allowed us to detect 100 ppbV NO_2 in ambient air with portable Raman equipment. Bao et al. recently reported a strategy for the detection of gaseous H_2S traces employing a plasmonic gold surface coated with an ultrathin CuO layer (≈2 nm).[12] H_2S reacted with CuO forming CuS, which was detectable by Raman. The dynamic range for H_2S detection was from 0.1 ppbV to 1 ppmV.

When molecules do not show any affinity for the plasmonic surface, the most common strategy for SERS detection is molecular trapping. To this purpose, porous materials may be used to concentrate gaseous molecules close to the surface, increasing the sensitivity of the SERS sensor. Metal−organic frameworks (MOFs), especially the zeolitic imidazolate frameworks (ZIF-8), are promising porous materials for SERS sensing applications due to their large specific surface area, hydrophobicity avoiding water interferences,[13] well-defined porous structure,[14] and tunable pore gate-opening.[15] The use of MOFs in SERS sensing was earlier proposed by the group of Van Duyne to detect vapors of benzene, toluene, nitrobenzene, or 2,6-di-*tert*-butylpyridine by molecular trapping on Ag "films-over-nanospheres" (AgFONs) using ZIF-8.[16] Following a similar approach, the group of Ling employed ZIF-8 films to trap toluene close to an array of Ag nanocubes reaching LOD of 200 ppmV.[17,18] In this case, the SERS substrates needed to equilibrate in a cell under static conditions and measured after 10 or 30 min. They were also able to detect 50 ppbV of 2-naphthalenethiol, a molecule with a much higher cross section and strong affinity by metal surfaces. Besides, Ling et al. demonstrated the sensor capabilities of remote detection but employing 4-methylbenzenethiol (4-MBT), again a model molecule with high cross section and strong metal affinity. Latest advances in the field of SERS-active nanoparticles/MOF hybrids have been recently reviewed by Wang et al.[19] Apart from the improved stability of the plasmonic nanostructures and the preconcentration effect of targets; additional synergistic effects due to the increased penetration depth of electromagnetic field at the metal/MOF interface and the superimposed charge-transfer mechanism between MOF and adsorbed molecules are drawing a very promising future.

The combined strategy of MOFs and the SERS technique is perfectly aligned with the growing demand for more generic and versatile gas sensing platforms for hazardous compounds. However, additional efforts, on the preparation of homogeneous MOF-based SERS substrate, with uniform, accurate, rapid, and repeatable SERS response toward target analytes, in real samples, are still required. For this purpose, we develop an ultrasensitive and reliable sensing platform based on a ZIF-8-coated Au@Ag nanorod (Au@Ag@ZIF-8) thin film with integrated Raman internal standard for rapid and quantitative SERS detection of trace CWA surrogates (Scheme 1). The

https://doi.org/10.1021/acssensors.1c00178
ACS Sens. 2021, 6, 2241−2251

SERS performance of the plasmonic platform is thoroughly analyzed using DMMP as a model neurotoxic simulant. First, we perform semiempirical and DFT calculations to investigate different aspects of the DMMP trapping inside the ZIF-8 cell as well as the type of interactions occurring between DMMP and Ag surface. Then, using a wide range of concentrations, from 2500 ppbV down to 50 ppbV, we determine the response time and limit of detection of the Au@Ag@ZIF-8 thin film. The recyclability of the substrate together with the effects of aging is also studied. Finally, in an attempt to evaluate the potential adoption of the platform in practical applications, preliminary results obtained with handheld Raman equipment for detection of DMMP in ambient air as well as for 2-chloroethyl ethyl sulfide (CEES, simulant of mustard agent) in nitrogen are discussed.

EXPERIMENTAL SECTION

Materials. Hexadecyltrimethylammonium bromide (CTAB, 98%), gold(III) chloride trihydrate ($HAuCl_4{\cdot}6H_2O$, 99.9%), hexadecyltrimethylammonium chloride solution (CTAC, 25 wt %), silver nitrate ($AgNO_3$), hydroquinone, sodium borohydride (99%), L-(+)-ascorbic acid, 2-methylimidazole (2-MeIm, 99%), zinc nitrate hexahydrate ($Zn(NO_3)_2{\cdot}6H_2O$, 99%), methanol dimethyl methylphosphonate (DMMP, 97%), 2-chloroethyl ethyl sulfide (CEES), and Tedlar gas sampling bags were purchased from Sigma-Aldrich. Milli-Q water (18.2 MΩ cm^{-1}) was used in all of the preparations. Polished SiO_2/Si wafers (4″; wet thermal oxide, 1 μm thick) were purchased from Sil′Tronix.

Synthesis of Au Nanorods. Au nanorods were synthesized following a previously reported seedless method using hydroquinone as a reducing agent.[20] Briefly, $HAuCl_4$ (0.4 mM, final concentration), $AgNO_3$ (0.26 mM, final concentration), and hydroquinone (5.26 mM, final concentration) were sequentially added into 74.6 mL of CTAB solution (0.1 M) under slight shaking. Then, $NaBH_4$ (1.7 μM) was added and kept standing overnight at 30 °C inside an incubator.

Synthesis of Au@Ag Core−Shell Nanorods. Au@Ag core−shell nanorods were synthesized following a previously reported method with slight modifications.[21] The as-prepared Au nanorods (10 mL) were washed (8000 rpm, 20 min) three times with 10 mL of CTAC (80 mM) and resuspended in 40 mL with CTAC (80 mM). Next, L-(+) ascorbic acid (7.45 mM) and $AgNO_3$ (0.745 mM) were sequentially added under stirring and kept standing for 3 h in an oven at 60 °C. The resulting Au@Ag nanorods were centrifuged three times (7000 rpm, 20 min) resuspending the pellet in 10 mL of H_2O (final CTAC concentration, ca. 0.6 mM).

Single Encapsulation of Metal Nanoparticles within ZIF-8. The individual coating of Au@Ag nanorods with ZIF-8 was based on a previously reported protocol with some modifications.[22] Typically, 0.144 mL of CTAB (1 mM) was added to 1 mL of an aqueous solution of 2-methylimidazole (1.32 M). The solution was stirred for 5 min and then 1 mL of $Zn(NO_3)_2{\cdot}6H_2O$ (24 mM) and 1 mL of Au@Ag nanorods were sequentially added under vigorous stirring. After 5 min of further magnetic stirring, the solution was left undisturbed for 3 h. The resulting core−shell Au@Ag@ZIF-8 nanoparticles were centrifuged twice (5000 rpm, 5 min). The resulting pellets were resuspended first in 10 mL of methanol and finally in 3.14 mL of methanol.

Synthesis of Pure ZIF-8 Nanoparticles. In a typical synthesis, cubic ZIF-8 nanoparticles were prepared by adding 30 mL of $Zn(NO_3)_2{\cdot}6H_2O$ (24 mM) and 30 mL of CTAB (0.5 mM) to 30 mL of 2-methylimidazole (1.32 M) under vigorous stirring. After 2 h standing, the resulting ZIF-8 nanoparticles were washed once with methanol and resuspended in 40 mL of methanol.

Preparation of SERS Substrates. Before the deposition of nanoparticles, the SiO_2/Si substrate (0.4 × 0.8 cm^2 area) was sequentially washed for 10 min in acetone, isopropanol, and water in an ultrasound bath and dried under N_2 stream. Then, Au@Ag@ZIF-8 nanoparticles were deposited onto the substrate by spin-coating the colloidal dispersion. It was carried out in two steps: (i) 30 s at 500 rpm and (ii) 60 s at 1000 rpm. Before starting each spin-coating step, 30 μL of colloids was drop-cast onto the substrate. The process was repeated three times.

SERS Detection of Gaseous DMMP. SERS measurements were conducted in a microfluidic gas chamber (2.7×10^{-2} cm^3), where a N_2 gas stream of 10 mL/min, with the desired concentration of DMMP, was fed continuously.[4,10] A gaseous stream of DMMP in nitrogen (2.5 ppmV, 12.7 mg/Nm^3) was generated using a calibrated permeation tube (MT-PD-Experimental 107-100-7845-HE3-C50, 126.78 ± 4.81 ng/min at 80 °C, from VALCO) immersed in a thermostatic bath at a controlled temperature (80 °C). In the case of lower concentrations of DMMP, Tedlar gas sampling bags were used. A stock bag of DMMP (11.3 ppmV, 57.3 mg/Nm^3) was prepared in N_2. For that purpose, 0.5 μL of DMMP was injected in 10 L of N_2 followed by homogenization. DMMP bags with concentrations of 900 ppbV (4.6 mg/Nm^3), 500 ppbV (2.5 mg/Nm^3), 250 ppbV (1.3 mg/Nm^3), 100 ppbV (0.5 mg/Nm^3), and 42.5 ppbV (0.2 mg/Nm^3) were prepared by step-by-step dilutions with N_2. Schemes of the experimental setup are shown in Supporting Information Figure S1.

SERS Detection of Gaseous CEES. SERS measurements were conducted in the same microfluidic gas chamber as DMMP. A gaseous stream CEES in nitrogen was generated through a diffusion vial type A (cross-sectional area of capillary, 0.19 cm^2; length of the diffusion path, 7.3 mm, from VICI) filled with pure CEES. The whole system was immersed in a thermostatic bath at a controlled temperature (20 °C). Considering the gas diffusion coefficient of 1.07×10^{-4} cm^2/s,[23] and linear driving force model, the CEES permeation rate and concentration were 3.9 ng/min and 76 ppbV (0.4 mg/Nm^3), respectively.

Characterization. Transmission electron microscopy (TEM) analysis was performed in a JEOL JEM 1010 microscope operating at an acceleration voltage of 100 kV to characterize the Au@Ag@ZIF-8 nanoparticle size and morphology. Scanning electron microscopy (SEM, CSEM-FEG Inspect) images operating at 20 kV were used to characterize the Au@Ag@ZIF-8 thin film. The UV−vis-NIR spectra of Au@Ag@ZIF-8 NPs and Au@Ag@ZIF-8 thin films on glass were acquired in either Agilent 8453 or Varian Cary 50 spectrometer. Nitrogen physisorption isotherms of ZIF8 nanoparticles were measured on ASAP 2020 V3.00 H to assess the surface area, pore volume, and pore size distribution. The sample was degassed at 13.3 kPa and 300 °C for 8 h.

SERS Characterization. SERS measurements were carried out using a confocal benchtop WITec Alpha 300 (spectral resolution 2 cm^{-1}) and a portable Raman BWTEK i-Raman Pro (spectral resolution 6 cm^{-1}, spot size 100 μm). Both equipment are coupled to a 785 nm laser, and all measurements were made in backscattering configuration. The measurements with WITec equipment were recorded with a 1.5 mW laser power, exposure time of 1 s, and a 20× objective (spot diameter, 1.92 μm; 0.52 mW/μm^2). Unless otherwise noted, SERS mappings of 50 × 50 μm^2 with 100 excitation spots were performed for each condition/experiment. SERS mappings provide a robust methodology for SERS quantification avoiding photodecomposition of both Ag@Au@ZIF-8 thin film and analyte. The SERS spectra recorded with the portable Raman were measured with 0.044 mW/μm^2 and an integration time of 40 s. Each single spectrum corresponds to the average of five spectra acquired in different points of the Au@Ag@ZIF-8 thin film.

Theoretical Calculations. The conformational analysis and the Raman spectra of DMMP were obtained theoretically using the M062X/6-311G** density functional method (DFT) as implemented in the Gaussian09 program, and the vibrational assignments were performed using the VEDA program. The adsorption of DMMP on the metallic nanoparticle and its corresponding Raman spectrum was studied by means of DFT calculations using a DMMP molecule adsorbed on silver sheets and clusters with different number of atoms as model. The interactions between DMMP and ZIF-8 at the molecular level were studied employing PM7 semiempirical computations as included in MOPAC2016 considering models of

https://doi.org/10.1021/acssensors.1c00178
ACS Sens. 2021, 6, 2241−2251

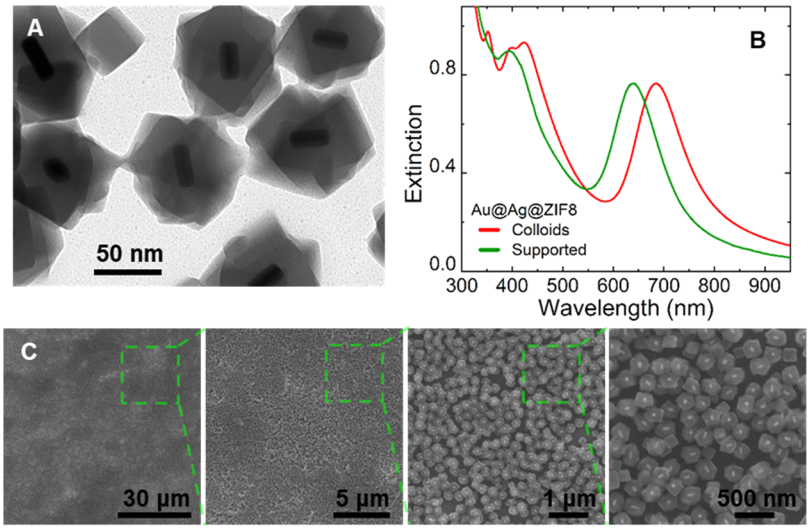

Figure 1. Analysis of Au@Ag@ZIF8 nanoparticles and thin films. (A) Representative TEM image Au@Ag@ZIF8 nanoparticles. (B) Extinction spectra of Au@Ag@ZIF8 colloids (red line) and Au@Ag@ZIF8 deposited onto SiO_2/Si substrate (green line). (C) Representative SEM images at different magnifications of an Au@Ag@ZIF-8 thin film prepared by spin coating.

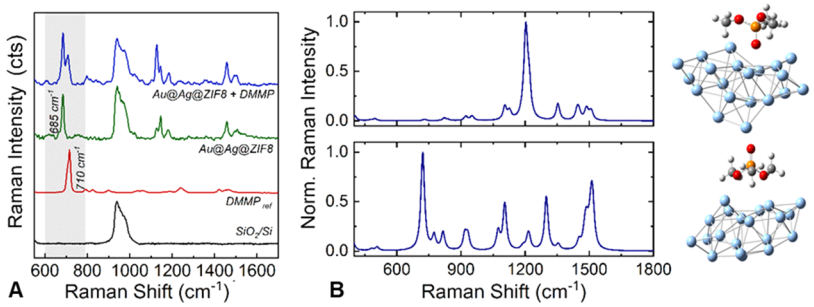

Figure 2. Analysis of the Raman and SERS spectra of DMMP. (A) SERS spectrum of 2.5 ppmV DMMP in N_2, recorded over Au@Ag@ZIF-8 thin films. The Raman spectra of SiO_2/Si substrate and DMMP in liquid phase and the SERS spectrum of Au@Ag@ZIF-8 thin film are also included as references. For better visualization, the spectra are depicted as a stack plot. (B) Calculated Raman spectra for Ag_{20}−DMMP complexes for the orientations (A) and (B), depicted on the right panel. Raman measurement conditions: 785 nm, 1.5 mW, and 1 s.

ZIF-8 of different sizes. Further details of these computations are included in Supporting Information Sections S3−S5.

Theoretical isotherm adsorption data for DMMP in ZIF-8 structure at 298 K were calculated by the combination of Monte Carlo (MC) simulations using the Metropolis−Hastings algorithm[24] and a molecular dynamics calculation based on UFF[25] as a force field. An optimization study was carried out to find the optimal parameters that provide the best results, specifically, 40 000 steps and 6 000 000 of equilibration points per step.

RESULTS AND DISCUSSION

Preparation and Characterization of Au@Ag@ZIF-8 Thin Films. Au@Ag@ZIF-8 nanoparticles consisting of a plasmonic core−shell Au@Ag nanorod coated with a ZIF-8 shell are obtained by CTAB-induced single encapsulation of the Au@Ag nanoparticles (81 ± 5 nm × 33 ± 2 nm; Figure S2 in the Supporting Information) within the MOF framework.[26,27] Figure 1A shows the representative TEM images of Au@Ag@ZIF-8 nanoparticles. The average Au@Ag@ZIF-8 nanoparticle size is 241 ± 25 nm with a ZIF-8 shell thickness of 90 ± 17 nm as determined from statistical analysis of TEM images (Figure S2C in the Supporting Information). As shown in Figure 1B, Au@Ag@ZIF-8 colloids exhibit the dipole plasmon modes centered at 700 and 440 nm, which can be attributed to the longitudinal and transversal localized surface plasmon resonances (LSPR) of Au@Ag nanorods, respectively. Additionally, other optical features are also evidenced at higher energies that could be ascribed to high-order modes.

The SERS substrates are prepared by spin-coating the Au@Ag@ZIF-8 colloids in methanol onto flat SiO_2/Si substrates. The optimization of the spin-coating process allows us to obtain uniform thin films with close-packed Au@Ag@ZIF-8 nanoparticles homogeneously distributed over the whole substrate (Figure 1C). The surface coverage estimated by ImageJ analysis of several SEM micrographs is 60 ± 8%. This value is in the same range as previously obtained with the Langmuir−Blodgett deposition technique.[28] The film uniformity is crucial for achieving good SERS performance in terms of reproducibility, reliability, and quantitative analysis. Figure 1B shows the optical response of the Au@Ag@ZIF-8 thin film. As expected, the optical features in the supported film are blue-shifted with respect to those ones observed in the colloidal dispersion due to changes in the refractive index of the surrounding medium (air vs methanol).

Analysis of the Raman and SERS Spectra of DMMP. The SERS performance of the Au@Ag@ZIF-8 thin films is analyzed using DMMP as a model analyte (Figure S3 in the Supporting Information), a simulant of gas Sarin. DMMP is a Raman-active molecule exhibiting several characteristic Raman peaks, among which dominates the peak centered at 718 cm^{-1}

https://doi.org/10.1021/acssensors.1c00178
ACS Sens. 2021, 6, 2241−2251

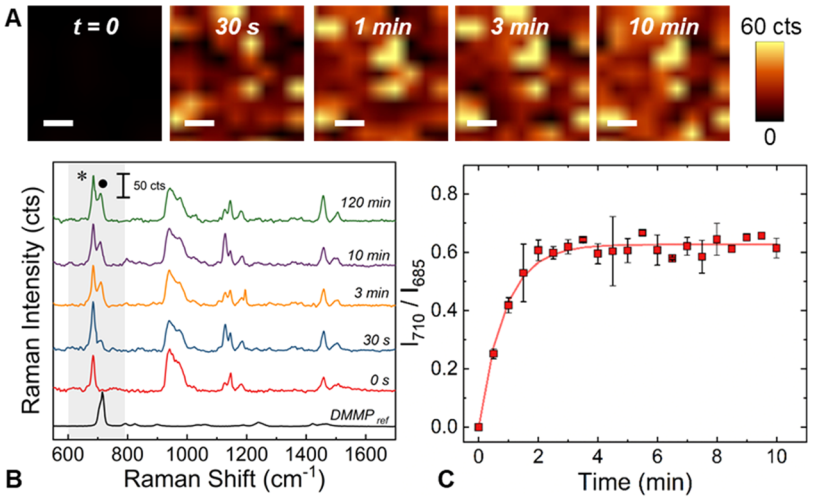

Figure 3. Time-resolved SERS detection of gaseous 2500 ppbV DMMP in N_2 using Ag@Au@ZIF-8 thin film as a sensing platform. (A) Representative SERS intensity mappings acquired at 710 cm^{-1} at different exposure times to 2500 ppbV DMMP in N_2. Scale bar represents 10 μm. (B) Average SERS spectra obtained from SERS mappings at different exposure times. The Raman spectrum of neat DMMP in liquid phase has been included as a reference. Gray-marked zone indicates the main vibrational modes of DMMP (710 cm^{-1}, marked with ●) and ZIF-8 (685 cm^{-1}, marked with *). For better visualization, the spectra have been displaced along the *y*-axis. (C) SERS intensity ratio between the intensity at 710 cm^{-1} (DMMP) and the intensity at 685 cm^{-1} (ZIF-8), I_{710}/I_{685}, as a function of exposure time to 2500 ppbV of DMMP in N_2. Each point in this graph represents the averaged value obtained from six different Ag@Au@ZIF-8 substrates. Adsorption kinetics was adjusted following the Lagergren equation. Raman measurement conditions: 785 nm, 1.5 mW, and 1 s.

(Figure S4 in the Supporting Information). For the complete assignment of DMMP Raman peaks, we perform DFT calculations (Figures S3 and S4, and Tables S1 and S2 in the Supporting Information). As shown in Figure S4 in the Supporting Information, the experimental and calculated Raman spectra show an excellent agreement in the fingerprint region between 400 and 1800 cm^{-1}. Accordingly, with our computed potential energy distribution (Tables S1 and S2 in the Supporting Information), the intense band at 718 cm^{-1} can be assigned to a combined vibrational mode involving the symmetrical stretching of the P−C bond and the two single P−O bonds. The two bands at lower wavenumbers, 466 and 504 cm^{-1}, can be assigned to O═PO and PO_3 bending modes, respectively, and the bands at 794 and 825 cm^{-1} would correspond to P−O and P−C asymmetric stretching. The isolated signal at 903 cm^{-1} can be assigned to a PCH_3 bending, while the broad bands around 1039 and 1062 cm^{-1} would be associated with the asymmetric and symmetric O−C stretchings, respectively. Besides, the theoretical computations predict a group of signals due to different O−CH_3 bendings, which would correspond to the experimental band at 1183 cm^{-1}. Finally, the signal at 1240 cm^{-1} is assigned mostly to the P═O stretching and the broad signals at 1419 and 1464 cm^{-1} to bendings of the methyl groups bonded to the P and O atoms, respectively.

SERS spectrum of DMMP in N_2 was recorded in a microfluidic gas chamber using the Au@Ag@ZIF-8 thin film as the sensing platform (Figure 2A). The presence of the characteristic signals of DMMP in the acquired SERS spectrum indicates that the DMMP can diffuse inside the ZIF-8 crystal to reach the plasmonic surface. Since the DMMP does not show any functional group sensitive (such as thiols or amines) to react covalently with Ag, we believe that it is simply physisorbed to the metal surface. To further confirm this observation, we simulate the Raman spectrum of DMMP adsorbed on a Ag surface. Initial calculations on the adsorption energy for different relative orientations of DMMP adsorbed on Ag sheets and clusters with different number of atoms, modeling the ⟨111⟩ silver surface, are performed (see Figures S5−S7 and Tables S3 and S4 in the Supporting Information). The calculated data indicate (Table S3 in the Supporting Information) that DMMP can be adsorbed on the Ag nanoparticle mainly in two orientations (Figure 2B), that is, with the oxygen atom of the P═O bond oriented directly to the space between adjacent silver atoms (orientation A) or interacting with the surface through the oxygen atoms of −OCH_3 groups (orientation B). The theoretical adsorption energies for these arrangements are quite similar, the former being only slightly 5 kcal/mol more favorable than the latter (around 20 vs 15 kcal/mol). Nevertheless, the comparison between the theoretical Raman spectra of Ag−DMMP complexes in favorable configurations and the experimental data (see Figure 2) shows that the best agreement is found for orientation B (further details in Figures S5−S7 and Tables S3 and S4 in the Supporting Information). The Raman spectrum for this orientation is dominated by the 710 cm^{-1} signal (see Figure 2B), which is also present in the experimental SERS spectrum (Figure 2A). Therefore, it can be concluded that adsorption of DMMP on the metal surface mainly occurs through interactions with the oxygen atoms in the −OCH_3 groups, as previously observed for Ag plates.[4]

Diffusion and trapping of DMMP within the ZIF-8 crystal suggest the existence of favorable molecular interactions between both species. To investigate it further, we perform computational studies (see Tables S5−S7 in the Supporting Information) using different models for the adsorption of DMMP on the ZIF-8 facets delimited by four or six zinc atoms (see Tables S5 and S6 in the Supporting Information). The results confirm that DMMP can be included within the ZIF-8 cavity and tends to be located closer to the facets formed by six Zn atoms with the oxygen atom of the P═O unit oriented toward the center of the facet or with the oxygen atoms of the methoxy groups oriented to the center (see Table S7 in the Supporting Information). In both conformations, steric

https://doi.org/10.1021/acssensors.1c00178
ACS Sens. 2021, 6, 2241−2251

repulsions between DMMP and the imidazole groups are minimized and stabilizing interactions with the oxygen atoms in the P═O and −O−CH_3 units are possible. The calculated adsorption energies for these interactions account for 23 kcal/mol. These values are within the same order of magnitude as the condensation enthalpy of DMMP molecules, i.e., 13 kcal/mol; in agreement with a DMMP physisorption process on ZIF-8.

The other significant features evidenced in the SERS spectrum of DMMP in N_2 (Figure 2A) can be attributed to the Au@Ag@ZIF-8 thin-film substrate. Thus, the broad peak around 900−1000 cm^{-1} can be assigned to SiO_2/Si substrate and peaks at 685, 1142, 1161, and 1488 cm^{-1} to the imidazolium ring, C−N stretching, and C−H stretching of ZIF-8, respectively.[29,30] Interestingly, the intense ZIF-8 peak at 685 cm^{-1} can act as a Raman internal standard since it does not overlap with the SERS signal of the DMMP. This internal standard, as shown below, will allow us to correct variations in the SERS signals improving the precision and accuracy of quantitative analysis.[31] A similar normalization approach has been recently applied for benzaldehyde measurements in the ppb range using Ag@ZIF-8 nanostructures.[32]

Detection Capabilities of Au@Ag@ZIF-8 Thin Films for Gaseous Neurotoxic Agents: Response Time, Sensitivity, and Limit of Detection. The sensing performance of Au@Ag@ZIF-8 thin films is tested by analyzing their SERS response as a function of exposure time to 2.5 ppmV DMMP in N_2. Figure 3A represents the Raman intensity mappings (50 × 50 μm^2, 100 spots) at 710 cm^{-1} for different exposure times. The uniformity of the SERS signal indicates the homogeneous distribution of hotspots over the two-dimensional (2D) Au@Ag@ZIF-8 substrate. The presence of DMMP is evidenced after 30 s of exposure, and it increases with time, as also evidenced in Figure 3B.

To accurately evaluate DMMP adsorption kinetics, SERS mappings of 100 μm^2 at 16 excitation spots were acquired every 30 s within the first 10 min. Since DMMP detected is directly related to the amount of molecules adsorbed from the gas phase on the microporous ZIF-8 layer,[16] the peak intensity of ZIF-8 at 685 cm^{-1} (I_{685}) can be used to normalize the SERS intensity of DMMP at 710 cm^{-1} (I_{710}). Figure 3C shows the time-dependent evolution of the averaged intensity ratio I_{710}/I_{685}. Each point in the graph represents the averaged I_{710}/I_{685} value and its standard deviation resulting from six different Ag@Au@ZIF-8 substrates. The average standard deviation is as low as 6%, which indicates the good responsiveness of the Ag@Au@ZIF-8 thin films in terms of substrate reproducibility, measurement repeatability, and homogeneity. Besides, in Figure 3C, it can be observed that the intensity and density of the SERS signal increase during the first 3 min and then stabilize once the equilibrium adsorption of the DMMP molecules on the Au@Ag@ZIF-8 porous substrate is established. The data are fitted to a Lagergren pseudo-first-order adsorption kinetic model[17] given as

$$I = I_{max}(1 - e^{-kt}) \quad (1)$$

where I is I_{710}/I_{685} at time t, I_{max} is the final SERS intensity ratio at pseudo-equilibrium conditions, and k (s^{-1}) is the pseudo-first-order adsorption rate constant. The obtained k, 1.9×10^{-2} s^{-1}, is in the same order of magnitude as that found by Phan-quang et al.[18] ($k = 5.5 \times 10^{-2}$ s^{-1}) for the detection of aerosolized 4-methylbenzenethiol (4-MBT). In addition, the SERS signal is stable even after 120 min feeding DMMP to the gas chamber (Figure S8 in the Supporting Information). Similar kinetic constants are obtained from the time-resolved SERS analyses of DMMP in N_2 within a concentration range of 50 to 2500 ppbV (see Figures S9 and S10, and Table S8 in the Supporting Information).

The early detection is vital to alert the population before the exposure to acute levels of concentration. In this work, we consider the response time as the time to reach 50% of the final I_{710}/I_{685} equilibrium value ($t_{50\%}$). In this particular case, detection with the benchtop equipment of 2500 ppbV DMMP in N_2 using Ag@Au@ZIF-8 thin film estimated $t_{50\%}$ at 41 s.

Next, the sensitivity of the Ag@Au@ZIF-8 thin film is tested by monitoring the SERS response as a function of the DMMP concentration ranging from 50 to 1000 ppbV. In Figure 4A, the

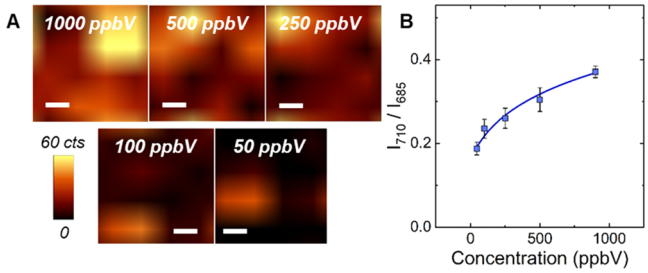

Figure 4. Sensitivity of Ag@Au@ZIF-8 substrate. (A) SERS mapping at 710 cm^{-1} recorded on Ag@Au@ZIF-8 substrates as a function of DMMP concentration after an exposure time of 10 min. Scale bar represents 10 μm. (B) I_{710}/I_{685} as a function of DMMP concentration. Each point in the graph corresponds to the average value of at least six mapped areas (50 × 50 μm^2, 100 spots) for the same Ag@Au@ZIF-8 substrate. The data were adjusted following the Freundlich equation. The error bar indicates the standard deviation. Raman measurement conditions: 785 nm, 1.5 mW, and 1 s.

SERS mappings acquired at 710 cm^{-1} show a gradual intensity decrease when the concentration of DMMP is reduced, which indicates a lower number of molecules adsorbed on the ZIF-8 matrix and, consequently, in close contact with the plasmonic surface. This observation is in accordance with the sticking probability dependence with concentration.[33] Regardless of the concentration of DMMP in N_2, the adsorption equilibrium is completely achieved after 10 min of exposure (see Figure S10 in the Supporting Information). The adsorption of gases on microporous ZIF-8[34] has been previously described using the Freundlich gas adsorption isotherm model

$$q = K_F P^{(1/n)} \quad (2)$$

where q is the total amount adsorbed, K_F and n are the Freundlich isotherm equation parameters, and P is the partial pressure of the gas. If we consider that q is directly proportional to the SERS intensity ratio I_{710}/I_{685}

$$I_{710}/I_{685} = k_f C^{(1/n)} \quad (3)$$

where C corresponds to the concentration expressed in ppbV. Considering this, our data are fitted to eq 3 obtaining $k_f = 7.9$ 10^{-2} and $n = 4.4$ ($R^2 = 0.98$) (Figure 4B). According to this calibration curve, the limit of detection (LOD)[35] obtained for the Ag@Au@ZIF-8 sensor corresponds to 0.2 ppbV (see Limit of Detection in the Supporting Information). This value is notably below AEGL-1 of sarin gas (1.2 ppbV). As far as we concern, this is the lowest detection value reported for nerve CWAs.

https://doi.org/10.1021/acssensors.1c00178
ACS Sens. 2021, 6, 2241−2251

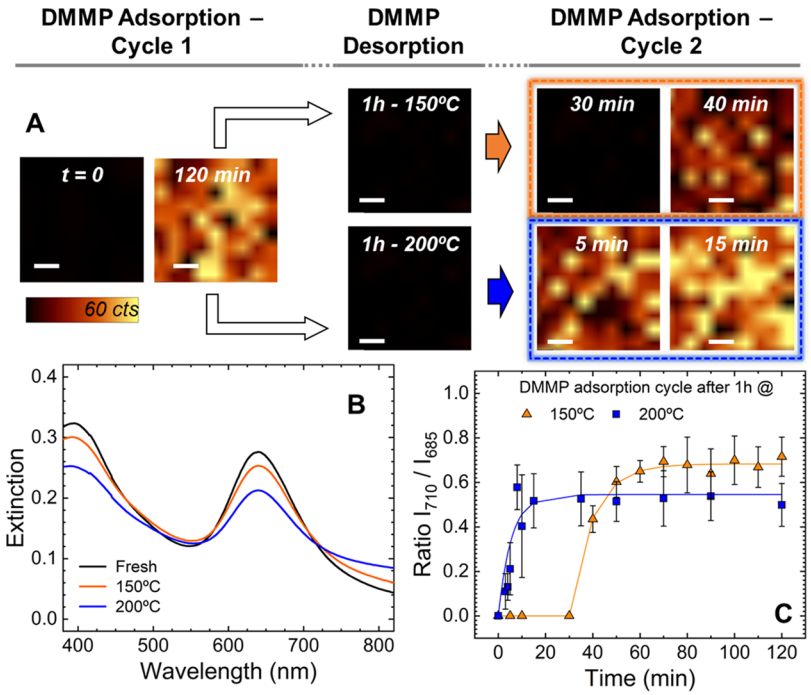

Figure 5. Reusability of Au@Ag@ZIF-8 thin films. (A) SERS mappings acquired at 710 cm^{-1} on Au@Ag@ZIF-8 thin films during the first DMMP adsorption cycle at 0 s and 120 min, after 1 h thermal treatment at 150 and 200 °C (DMMP desorption), and during the second DMMP adsorption cycle at 30 and 40 min for Au@Ag@ZIF-8 thin films treated at 150 °C and at 5 and 15 min for those treated at 200 °C. Scale bars indicate 10 μm. (B) Extinction spectra of Au@Ag@ZIF-8 thin films before and after thermal annealing at 150 and 200 °C. (C) Average SERS intensity ratio (I_{710}/I_{685}) as a function of exposure time obtained for the second cycle of 2.5 ppmV DMMP adsorption employing Au@Ag@ZIF-8 thin films treated at 150 °C (triangles) and 200 °C (squares). The error bar indicates the standard deviation of data obtained from three different Au@Ag@ZIF-8 thin films. Raman measurement conditions: 785 nm, 1.5 mW, and 1 s.

Next, the regeneration and reusability of the Au@Ag@ZIF-8 thin films are investigated. Since it implies the desorption of all DMMP molecules adsorbed either within the micropores of ZIF-8 or on the metal surface, first, we identified the degassing temperature from thermogravimetric analysis (TGA) using pure ZIF-8 nanoparticles (Figure S11 in the Supporting Information). Figure S12 in the Supporting Information shows the differential TGA profiles of pure ZIF-8 crystals before and after saturation with DMMP vapor at 20 °C (ca. 700 ppmV) in a glass vial. By subtracting the weight loss of the control sample, i.e., pure ZIF-8 before exposure to toxic vapors, a DMMP sorption capacity of 83 mg/g was estimated for the ZIF-8. Moreover, the differential thermogravimetric analysis reveals that the desorption peak of DMMP is centered at 120 °C and total DMMP desorption takes place at around 200 °C, confirming that thermal annealing can be a suitable approach to regenerate Au@Ag@ZIF-8 thin films. It is also worthy to mention that the normal boiling point of DMMP, i.e., 181 °C, fits within this temperature region, in agreement with a DMMP physisorption process on ZIF-8. Nevertheless, we have to consider that thermal annealing could induce the reshaping of Au@Ag nanorods and therefore the loss of sensing capabilities of the Au@Ag@ZIF-8 thin films. To avoid any damage to the nanostructures during the regeneration process, we investigate the effects of thermal annealing (1 h) at 150 and 200 °C in the performance of Au@Ag@ZIF-8 substrates when reused. For doing that, first, the Au@Ag@ZIF-8 thin films are exposed to one cycle of 2.5 ppmV DMMP adsorption for 120 min. As expected, the SERS analysis of the substrates reveals that DMMP is uniformly distributed along the whole plasmonic substrates (Figure 5A). Next, the Au@Ag@ZIF-8 thin films are heated at 150 or 200 °C for 1 h and then characterized by SEM, UV−vis, and Raman spectroscopies. Figure 5B shows the extinction spectra of the Au@Ag@ZIF-8 thin films before and after the thermal treatment where almost no changes in the LSPR response of the Au@Ag@ZIF-8 substrates are observed at 150 °C and slight changes at 200 °C. Moreover, no morphological changes in the Au@Ag@ZIF-8 nanoparticles are evidenced during the SEM analysis of plasmonic substrates (Figure S13 in the Supporting Information). Additionally, we analyze the reusability carrying out a second cycle of DMMP detection using the Au@Ag@ZIF-8 thin films annealed at 150 and 200 °C. The time-resolved SERS analyses (Figure 5A,C) reveals that while no SERS signal of DMMP is observed up to 40 min of exposure for Au@Ag@ZIF-8 thin films treated at 150 °C, the presence of DMMP is detected after 5 min for those regenerated at 200 °C. Moreover, the kinetic constant k decreases to 3.0×10^{-3} from 1.9×10^{-2} s^{-1} obtained in the first cycle. This result may indicate that the diffusion of DMMP through the ZIF-8 pores is slowed down during the second cycle, maybe due to residual DMMP molecules still retained in the micropores or near the plasmonic Au@Ag surface.

Finally, the aging of the Au@Ag@ZIF-8 thin films is investigated. Thus, Au@Ag@ZIF-8 thin films are stored at room temperature and normal atmosphere after their preparation and analyzed as prepared and after 1 and 20 days. The aging of the Au@Ag@ZIF-8 thin film produces slight changes in the LSPR response (see Figure S14A). To investigate the effect of aging on the SERS performance, we analyze the detection of 2.5 ppmV DMMP in N_2 employing as-prepared and 20-day aged Au@Ag@ZIF-8 thin films. The time

https://doi.org/10.1021/acssensors.1c00178
ACS Sens. 2021, 6, 2241−2251

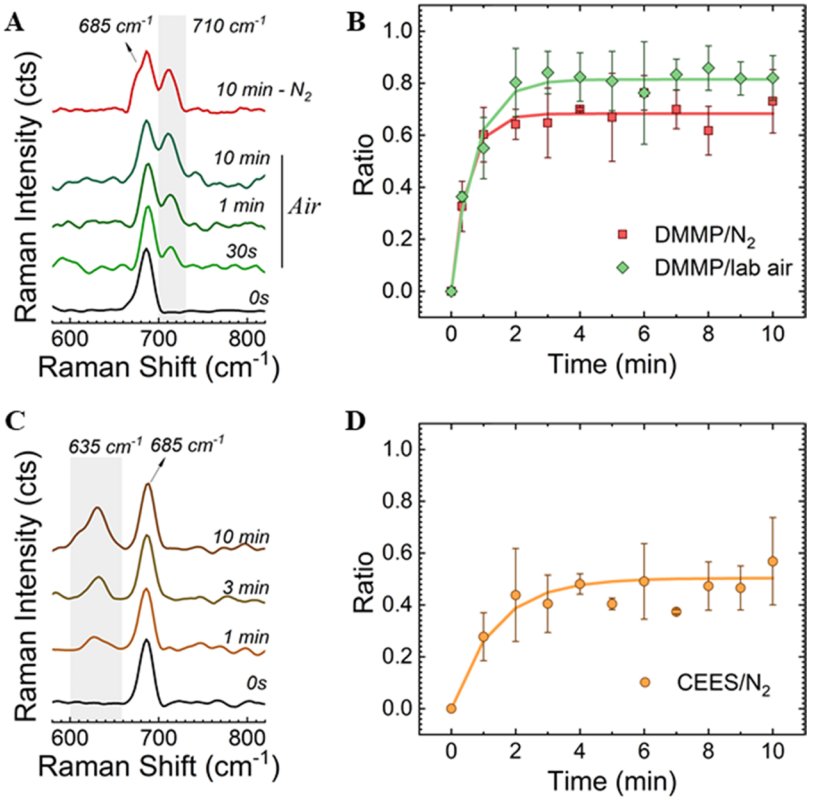

Figure 6. On-field detection capabilities of Ag@Au@ZIF-8 substrate using a portable Raman equipment. (A) Average SERS recorded as a function of exposure time to 2.5 ppmV of DMMP diluted in laboratory air compared with spectra of DMMP diluted in N_2 at 10 min. (B) SERS intensity ratio, I_{710}/I_{685}, as a function of exposure time to 2.5 ppmV of DMMP in air and N_2. (C) SERS spectra as a function of exposure time to 76 ppbV of CEES in N_2. (D) SERS intensity ratio, I_{635}/I_{685}, as a function of exposure time to 76 ppbV of CEES diluted in N_2. In (A) and (C), for a better visualization, the spectra have been displaced along the *y*-axis. In (B) and (D), the error bar indicates the standard deviation calculated using three different substrates and the adsorption kinetics are fitted to the Lagergren equation. Raman measurement conditions: 785 nm, 350 mW, and 40 s.

evolution of the SERS intensity ratio (I_{710}/I_{685}) is rather similar for as-prepared and 20-day aged plasmonic substrates (Figure S14B), indicating that the aging does not remarkably affect the substrates. In fact, the kinetic constant decreased from 1.9×10^{-2} to 1.0×10^{-2} s^{-1} Au@Ag@ZIF-8 thin films and the time to reach the equilibrium increased from 3 to 5 min. Finally, the response time $t_{50\%}$ is 87 s.

Performance of SERS Substrates for Chemical Warfare Agents (CWA) Gas-Phase Detection under Relevant Conditions. We have demonstrated so far that Au@Ag@ZIF-8 thin films show a fast response, low detection limit, possibility of regeneration, and long-term stability. In addition, when developing a gas monitoring system for a real application outside of laboratory, two important aspects need to be considered: (i) interferences present in ambient air and (ii) robust detection with portable devices.

To demonstrate the performance of Au@Ag@ZIF-8 thin films in ambient air using a portable equipment, the SERS substrate is mounted inside a gas flow cell as shown in the experimental setup in Figure S15 in the Supporting Information. The experiment is performed using 2.5 ppmV DMMP in ambient air coming directly from the laboratory to add common interferences such as carbon dioxide, water, and possibly volatile organic compounds present in the lab indoor air. Figure 6A shows SERS spectra as a function of exposure time to DMMP in laboratory air, together with the DMMP SERS spectrum in N_2 after 10 min. The fact that SERS signals are broader than those one acquired with a bench equipment (Figures 2A and 3B) is due to the lower spectral resolution of the portable equipment. The time-resolved SERS analysis shows that DMMP is detected after just 30 s. Besides, the spectrum of DMMP in N_2 clearly shows a lower signal-to-noise ratio due to the absence of impurities as well as lower intensity compared to the spectra in air. This lower intensity is clearly observed in Figure 6B, where SERS intensity ratio, I_{710}/I_{685}, as a function of exposure time is presented. In general, the effect of humidity significantly affects the performance of standard chemical sensors; nevertheless, in the presence of humidity, we observe an increase of the SERS intensity ratio I_{710}/I_{685}.[36] Taking into account that water is a very weak Raman scatterer, our hypothesis relies on the increase of the DMMP adsorption on ZIF-8 at low concentrations mediated by hydrogen-bond-type interactions with the co-adsorbed water molecules. This is corroborated through the simulation of adsorption isotherms for DMMP and the binary mixture DMMP and water. As shown in Figure S16 in the Supporting Information, the adsorption energy for DMMP is higher in the binary mixture, in spite of being a competitive adsorption process and the lower amount of adsorbed DMMP.

It is also worth noting that the average standard deviations obtained for DMMP sensing using three different Au@Ag@ZIF-8 substrates are 13 and 12% for DMMP in N_2 and laboratory air, respectively. Besides, the $t_{50\%}$ values measured with the portable equipment are 22 and 29 s for DMMP diluted in N_2 and laboratory air, respectively. These values are 6 times lower than the ones reported previously for the

https://doi.org/10.1021/acssensors.1c00178
ACS Sens. 2021, 6, 2241−2251

detection of 2.5 ppmV of DMMP with the same portable Raman equipment.[4] These response times open the door to use these SERS substrates in real scenario.

Finally, we also investigate the SERS detection of CEES molecule in N_2 in a portable equipment using Au@Ag@ZIF-8 thin films. The Raman spectrum of the pure CEES molecule shows three intense bands at 650 cm^{-1} (C−S−C stretching and C−S bending), 690 cm^{-1} (C−S stretching), and 750 cm^{-1} (C−Cl stretching) (Figure S17 in the Supporting Information). The SERS monitoring of the CEES detection with the portable equipment during the exposure of the plasmonic thin films to 76 ppbV CEES clearly reveals its characteristic peak after 1 min (Figure 6C). Likewise, for DMMP quantification, CEES Raman signal is also normalized using the intensity of ZIF-8 signal at 685 cm^{-1} (I_{685}). Figure 6D shows the time-dependent evolution of the I_{635}/I_{685} ratio upon exposure to 76 ppbV CEES in N_2. The data analysis allows us to estimate a response of 54 s and an average standard deviation of 22%, which is comparatively higher than the registered for DMMP exposure at 2.5 ppmV due to the less amount of target molecules in the gas phase. On the other hand, the average I_{635}/I_{685} ratio for CEES detection is in the same range, even at a concentration 100-fold lower. We attribute this effect to the irreversible chemisorption of CEES molecules in the vicinity of the enhancing metallic surface. These preliminary results demonstrate the potential of Au@Ag@ZIF-8 thin films for CEES detection in the operational window between the AEGL-1 and AEGL-2 values for 10 min exposure of sulfur mustard gas, which are 60 and 90 ppbV, respectively.[37]

CONCLUSIONS

We develop a SERS platform that consists of a thin film of core−shell Au@Ag@ZIF-8 nanoparticles, spin-coated on a SiO_2/Si wafer substrate. The homogeneity of the SERS substrate allows us to use the characteristic Raman peak of ZIF-8 at 685 cm^{-1} as the internal standard for quantitative detection. The SERS platform has been validated for the detection of DMMP, at concentrations between 50 ppbV to 2.5 ppmV in gas phase reaching a LOD of 0.2 ppbV. The response time ($t_{50\%}$) of the Au@Ag@ZIF-8 thin films remains lower than 1 min in all of the situations studied. The SERS substrate shows good stability after storage in a closed vial for 20 days, and it is possible to reuse it after regeneration by degassing at 200 °C. Importantly, Au@Ag@ZIF-8 thin films demonstrate good capabilities to detect 2.5 ppmV DMMP in ambient air using a portable Raman equipment with a response time of 21 s. Finally, experiments with another CWA such as CEES, surrogate of mustard gas, indicate that this sensing platform can be extended to the detection of other CWA. Thus, 76 ppbV of CEES were detected with a portable Raman equipment with a response time of 54 s. In general, the SERS performance parameters of our Au@Ag@ZIF-8 sensing platform match with the technical requirements for the early detection of CWAs in air according to the AEGL reference values. This proof of concept paves the way for further developments on SERS-based gas sensing in real applications as security and defense, healthcare and environmental monitoring, or agro-food industry.

ASSOCIATED CONTENT

Supporting Information

The Supporting Information is available free of charge at https://pubs.acs.org/doi/10.1021/acssensors.1c00178.

Experimental setup for the SERS detection of DMMP and CEES; morphological and optical characterization of Au@Ag nanorods; conformational analysis of DMMP and computational simulation of Raman spectrum of isolated DMMP; computational analysis of DMMP adsorption on silver and calculation of Raman spectra; computational analysis of the interactions between DMMP and ZIF-8; detection capabilities of Au@Ag@ZIF-8 thin films; limit of detection (LOD); adsorption characterization of ZIF-8 crystals; SEM characterization of Ag@Au@ZIF-8 substrate after heat treatment; analysis of the aging of Au@Ag@ZIF-8 substrates; experimental setup for portable detection; simulated adsorption isotherms; and Raman signature of CEES (PDF)

AUTHOR INFORMATION

Corresponding Authors

Isabel Pastoriza-Santos − *CINBIO, Universidade de Vigo, Departamento de Química Física, Campus Universitario Lagoas Marcosende, 36310 Vigo, Spain; Galicia Sur Health Research Institute (IIS Galicia Sur), 36310 Vigo, Spain;* orcid.org/0000-0002-1091-1364; Email: pastoriza@uvigo.es

Reyes Mallada − *Instituto de Nanociencia y Materiales de Aragón (INMA), CSIC-Universidad de Zaragoza, 50009 Zaragoza, Spain; Departamento de Ingeniería Química y Tecnologías del Medio Ambiente, Universidad de Zaragoza, 50018 Zaragoza, Spain; Networking Research Center on Bioengineering, Biomaterials and Nanomedicine, 28029 Madrid, Spain;* orcid.org/0000-0002-4758-9380; Email: rmallada@unizar.es

Authors

Marta Lafuente − *Instituto de Nanociencia y Materiales de Aragón (INMA), CSIC-Universidad de Zaragoza, 50009 Zaragoza, Spain; Departamento de Ingeniería Química y Tecnologías del Medio Ambiente, Universidad de Zaragoza, 50018 Zaragoza, Spain*

Sarah De Marchi − *CINBIO, Universidade de Vigo, Departamento de Química Física, Campus Universitario Lagoas Marcosende, 36310 Vigo, Spain; Galicia Sur Health Research Institute (IIS Galicia Sur), 36310 Vigo, Spain;* orcid.org/0000-0003-0536-8237

Miguel Urbiztondo − *Centro Universitario de la Defensa de Zaragoza, 50090 Zaragoza, Spain;* orcid.org/0000-0002-4931-1358

Ignacio Pérez-Juste − *CINBIO, Universidade de Vigo, Departamento de Química Física, Campus Universitario Lagoas Marcosende, 36310 Vigo, Spain*

Jesús Santamaría − *Instituto de Nanociencia y Materiales de Aragón (INMA), CSIC-Universidad de Zaragoza, 50009 Zaragoza, Spain; Departamento de Ingeniería Química y Tecnologías del Medio Ambiente, Universidad de Zaragoza, 50018 Zaragoza, Spain; Networking Research Center on Bioengineering, Biomaterials and Nanomedicine, 28029 Madrid, Spain;* orcid.org/0000-0002-8701-9745

María Pina − *Instituto de Nanociencia y Materiales de Aragón (INMA), CSIC-Universidad de Zaragoza, 50009 Zaragoza, Spain; Departamento de Ingeniería Química y Tecnologías del Medio Ambiente, Universidad de Zaragoza, 50018 Zaragoza, Spain; Networking Research Center on*

Bioengineering, Biomaterials and Nanomedicine, 28029 Madrid, Spain; orcid.org/0000-0001-9897-6527

Complete contact information is available at: https://pubs.acs.org/10.1021/acssensors.1c00178

Author Contributions

This manuscript was written through contributions of all authors. All authors have given approval to the final version of the manuscript.

Funding

The authors are grateful for financial support from the European Union's Horizon 2020 research and innovation programme under grant agreement no. 883390 (H2020-SU-SECU-2019 SERSing Project), Spanish State Research Agency (CTQ2016-79419-R, MAT2016-77809-R, PID2019-108660RB-I00 and PID2019-108954RB-I00), Gobierno de Aragón (T57-17R p, Feder 2014-2020 "Construyendo Europa desde Aragón"), Xunta de Galicia (GRC ED431C 2016-048, FEDER 1014-2020), and CIBER-BNN (initiative funded by the VI National R&D&i Plan 2008−2011, Iniciativa Ingenio 2010, Consolider Program, CIBER Actions, and financed by the Instituto de Salud Carlos III with assistance from the European Regional Development Fund).

Notes

The authors declare no competing financial interest.

■ ACKNOWLEDGMENTS

The authors acknowledge the use of Servicio General de Apoyo a la Investigación-SAI, Universidad de Zaragoza. They acknowledge Laboratorio de Microscopías Avanzadas-Universidad de Zaragoza for offering access to their instruments and expertise. S.D.M. acknowledges the support from CsF/CNPq-Brazil fellowship.

■ ABBREVIATIONS

AEGLs, acute exposure guideline levels; CEES, 2-chloroethyl ethyl sulfide; CWA, chemical warfare agents; DFT, density functional method; DMMP, dimethyl methylphosphonate; EPA, US Environmental Protection Agency; LBL, layer-by-layer; LOD, limit of detection; LSPR, localized surface plasmon resonances; MC, Monte Carlo simulations; MOF, metal−organic framework; SERS, surface-enhanced Raman scattering; TEM, transmission electron microscopy; TGA, thermogravimetric analysis; VOCs, volatile organic compounds; ZIF, zeolitic imidazolate framework

■ REFERENCES

(1) Langer, J.; Jimenez de Aberasturi, D.; Aizpurua, J.; Alvarez-Puebla, R. A.; Auguié, B.; Baumberg, J. J.; Bazan, G. C.; Bell, S. E. J.; Boisen, A.; Brolo, A. G.; et al. Present and Future of Surface-Enhanced Raman Scattering. *ACS Nano* **2020**, *14*, 28−117.

(2) Hakonen, A.; Wu, K.; Stenbæk Schmidt, M.; Andersson, P. O.; Boisen, A.; Rindzevicius, T. Detecting Forensic Substances Using Commercially Available SERS Substrates and Handheld Raman Spectrometers. *Talanta* **2018**, *189*, 649−652.

(3) Oh, M. K.; De, R.; Yim, S. Y. Highly Sensitive VOC Gas Sensor Employing Deep Cooling of SERS Film. *J. Raman Spectrosc.* **2018**, *49*, 800−809.

(4) Lafuente, M.; Sanz, D.; Urbiztondo, M. A.; Santamaría, J.; Pina, M. P.; Mallada, R. Gas Phase Detection of Chemical Warfare Agents CWAs with Portable Raman. *J. Hazard. Mater.* **2020**, *384*, No. 121279.

(5) *Agent GB (Sarin) Results - AEGL Program | Acute Exposure Guideline Levels for Airborne Chemicals |*, US EPA, https://www.epa.gov/aegl/agent-gb-sarin-results-aegl-program (accessed Apr 30, 2020).

(6) Christesen, S. D. Raman Cross Sections of Chemical Agents and Simulants. *Appl. Spectrosc.* **1988**, *42*, 318−321.

(7) Jiang, Y.; Sun, D. W.; Pu, H.; Wei, Q. Surface Enhanced Raman Spectroscopy (SERS): A Novel Reliable Technique for Rapid Detection of Common Harmful Chemical Residues. *Trends Food Sci. Technol.* **2018**, *75*, 10−22.

(8) Hakonen, A.; Andersson, P. O.; Stenbæk Schmidt, M.; Rindzevicius, T.; Käll, M. Explosive and Chemical Threat Detection by Surface-Enhanced Raman Scattering: A Review. *Anal. Chim. Acta* **2015**, *893*, 1−13.

(9) Lauridsen, R. K.; Rindzevicius, T.; Molin, S.; Johansen, H. K.; Berg, R. W.; Alstrøm, T. S.; Almdal, K.; Larsen, F.; Schmidt, M. S.; Boisen, A. Towards Quantitative SERS Detection of Hydrogen Cyanide at Ppb Level for Human Breath Analysis. *Sens. Bio-Sensing Res.* **2015**, *5*, 84−89.

(10) Lafuente, M.; Pellejero, I.; Sebastián, V.; Urbiztondo, M. A.; Mallada, R.; Pina, M. P.; Santamaría, J. Highly Sensitive SERS Quantification of Organophosphorous Chemical Warfare Agents: A Major Step towards the Real Time Sensing in the Gas Phase. *Sens. Actuators, B* **2018**, *267*, 457−466.

(11) Kim, S.; Kim, D. H.; Park, S. G. Highly Sensitive and On-Site NO_2 SERS Sensors Operated under Ambient Conditions. *Analyst* **2018**, *143*, 3006−3010.

(12) Bao, H.; Zhang, H.; Fu, H.; Zhou, L.; Zhang, P.; Li, Y.; Cai, W. Ultrathin Layer Solid Transformation-Enabled-Surface Enhanced Raman Spectroscopy for Trace Harmful Small Gaseous Molecule Detection. *Nanoscale Horiz.* **2020**, *5*, 739−746.

(13) Zhang, K.; Lively, R. P.; Zhang, C.; Chance, R. R.; Koros, W. J.; Sholl, D. S.; Nair, S. Exploring the Framework Hydrophobicity and Flexibility of Zif-8: From Biofuel Recovery to Hydrocarbon Separations. *J. Phys. Chem. Lett.* **2013**, *4*, 3618−3622.

(14) Zheng, B.; Sant, M.; Demontis, P.; Suffritti, G. B. Force Field for Molecular Dynamics Computations in Flexible ZIF-8 Framework. *J. Phys. Chem. C* **2012**, *116*, 933−938.

(15) Zheng, B.; Wang, L. L.; Du, L.; Huang, K. W.; Du, H. ZIF-8 Gate Tuning via Terminal Group Modification: A Computational Study. *Chem. Phys. Lett.* **2016**, *658*, 270−275.

(16) Kreno, L. E.; Greeneltch, N. G.; Farha, O. K.; Hupp, J. T.; Van Duyne, R. P. SERS of Molecules That Do Not Adsorb on Ag Surfaces: A Metal−Organic Framework-Based Functionalization Strategy. *Analyst* **2014**, *139*, 4073−4080.

(17) Koh, C. S. L.; Lee, H. K.; Han, X.; Sim, H. Y. F.; Ling, X. Y. Plasmonic Nose: Integrating the MOF-Enabled Molecular Preconcentration Effect with a Plasmonic Array for Recognition of Molecular-Level Volatile Organic Compounds. *Chem. Commun.* **2018**, *54*, 2546−2549.

(18) Phan-quang, G. C.; Yang, N.; Lee, H. K.; Yi, H.; Sim, F.; Sher, C.; Koh, L.; Kao, Y.; Wong, Z. C.; Khay, E.; et al. Tracking Airborne Molecules from Afar: Three-Dimensional Metal−Organic-Framework - Surface-Enhanced Raman Scattering (MOF-SERS) Platform for Stand-Off and Real-Time Atmospheric Monitoring. *ACS Nano* **2019**, *13*, 12090−12099.

(19) Huang, C.; Li, A.; Chen, X.; Wang, T. Understanding the Role of Metal−Organic Frameworks in Surface-Enhanced Raman Scattering Application. *Small* **2020**, *16*, No. 2004802.

(20) Zhang, L.; Xia, K.; Lu, Z.; Li, G.; Chen, J.; Deng, Y.; Li, S.; Zhou, F.; He, N. Efficient and Facile Synthesis of Gold Nanorods with Finely Tunable Plasmonic Peaks from Visible to Near-IR Range. *Chem. Mater.* **2014**, *26*, 1794−1798.

(21) Zhou, N.; Polavarapu, L.; Gao, N.; Pan, Y.; Yuan, P.; Wang, Q.; Xu, Q. H. TiO_2 Coated Au/Ag Nanorods with Enhanced Photocatalytic Activity under Visible Light Irradiation. *Nanoscale* **2013**, *5*, 4236−4241.

(22) Hu, P.; Zhuang, J.; Chou, L. Y.; Lee, H. K.; Ling, X. Y.; Chuang, Y. C.; Tsung, C. K. Surfactant-Directed Atomic to Mesoscale

Alignment: Metal Nanocrystals Encased Individually in Single-Crystalline Porous Nanostructures. *J. Am. Chem. Soc.* **2014**, *136*, 10561−10564.
(23) Singh, V. V.; Nigam, A. K.; Boopathi, M.; Pandey, P.; Singh, B.; Vijayaraghavan, R. In Situ Electrochemical Sensing of 2-Chloroethyl Ethyl Sulfide (CEES) a CWA Simulant Using CuPc/RTIL Composite Gold Electrode. *Sens. Actuators, B* **2012**, *161*, 1000−1009.
(24) Chib, S.; Greenberg, E. Understanding the Metropolis-Hastings Algorithm. *Am. Stat.* **1995**, *49*, 327−335.
(25) Rappe, A. K.; Casewit, C. J.; Colwell, K. S.; Goddard, W. A.; Skiff, W. M. UFF, a Full Periodic Table Force Field for Molecular Mechanics and Molecular Dynamics Simulations. *J. Am. Chem. Soc.* **1992**, *114*, 10024−10035.
(26) Zheng, G.; de Marchi, S.; López-Puente, V.; Sentosun, K.; Polavarapu, L.; Pérez-Juste, I.; Hill, E. H.; Bals, S.; Liz-Marzán, L. M.; Pastoriza-Santos, I.; et al. Encapsulation of Single Plasmonic Nanoparticles within ZIF-8 and SERS Analysis of the MOF Flexibility. *Small* **2016**, *12*, 3935−3943.
(27) De Marchi, S.; Vázquez-Iglesias, L.; Bodelón, G.; Pérez-Juste, I.; Ángel Fernández, L.; Pérez-Juste, J.; Pastoriza-Santos, I. Programmable Modular Assembly of Functional Proteins on Raman-Encoded Zeolitic Imidazolate Framework-8 (ZIF-8) Nanoparticles as SERS Tags. *Chem. Mater.* **2020**, *32*, 5739−5749.
(28) Lafuente, M.; Ruiz-Rincón, S.; Mallada, R.; Cea, P.; Pilar Pina, M. Towards the Reproducible Fabrication of Homogeneous SERS Substrates by Langmuir-Schaefer Technique: A Low Cost and Scalable Approach for Practical SERS Based Sensing Applications. *Appl. Surf. Sci.* **2020**, *506*, No. 144663.
(29) Kumari, G.; Jayaramulu, K.; Maji, T. K.; Narayana, C. Temperature Induced Structural Transformations and Gas Adsorption in the Zeolitic Imidazolate Framework ZIF-8: A Raman Study. *J. Phys. Chem. A* **2013**, *117*, 11006−11012.
(30) Pillai, P.; Dharaskar, S.; Sasikumar, S.; Khalid, M. Zeolitic Imidazolate Framework-8 Nanoparticle: A Promising Adsorbent for Effective Fluoride Removal from Aqueous Solution. *Appl. Water Sci.* **2019**, *9*, No. 150.
(31) Shen, W.; Lin, X.; Jiang, C.; Li, C.; Lin, H.; Huang, J.; Wang, S.; Liu, G.; Yan, X.; Zhong, Q.; et al. Reliable Quantitative SERS Analysis Facilitated by Core−Shell Nanoparticles with Embedded Internal Standards. *Angew. Chem., Int. Ed.* **2015**, *54*, 7308−7312.
(32) Yang, K.; Zong, S.; Zhang, Y.; Qian, Z.; Liu, Y.; Zhu, K.; Li, L.; Li, N.; Wang, Z.; Cui, Y. Array-Assisted SERS Microfluidic Chips for Highly Sensitive and Multiplex Gas Sensing. *ACS Appl. Mater. Interfaces* **2020**, *12*, 1395−1403.
(33) Biggs, K. B.; Camden, J. P.; Anker, J. N.; Duyne, R. P. V. Surface-Enhanced Raman Spectroscopy of Benzenethiol Adsorbed from the Gas Phase onto Silver Film over Nanosphere Surfaces: Determination of the Sticking Probability and Detection Limit Time. *J. Phys. Chem. A* **2009**, *113*, 4581−4586.
(34) Zhang, Z.; Xian, S.; Xi, H.; Wang, H.; Li, Z. Improvement of CO_2 Adsorption on ZIF-8 Crystals Modified by Enhancing Basicity of Surface. *Chem. Eng. Sci.* **2011**, *66*, 4878−4888.
(35) Massarini, E.; Wästerby, P.; Landström, L.; Lejon, C.; Beck, O.; Andersson, P. O. Methodologies for Assessment of Limit of Detection and Limit of Identification Using Surface-Enhanced Raman Spectroscopy. *Sens. Actuators, B* **2015**, *207*, 437−446.
(36) Qiao, X.; Su, B.; Liu, C.; Song, Q.; Luo, D.; Mo, G.; Wang, T. Selective Surface Enhanced Raman Scattering for Quantitative Detection of Lung Cancer Biomarkers in Superparticle@MOF Structure. *Adv. Mater.* **2018**, *30*, No. 1702275.
(37) *Sulfur Mustard Results - AEGL Program | Acute Exposure Guideline Levels for Airborne Chemicals* |, US EPA, https://www.epa.gov/aegl/sulfur-mustard-results-aegl-program (accessed Apr 30, 2020).

https://doi.org/10.1021/acssensors.1c00178
ACS Sens. 2021, 6, 2241−2251